[2]Dutton, J. C., and Addy, A. L., "Transonic Flow in the Throat Region of Annular Supersonic Nozzles," *AIAA Journal*, Vol. 19, No. 9, 1982, pp. 1236–1243.

[3]Carroll, B. F., and Dutton, J. C., "Transonic Flow in the Throat Region of Radial or Nearly Radial Supersonic Nozzles," *AIAA Journal*, Vol. 23, No. 7, 1985, pp. 1127–1129.

[4]Carroll, B. F., Hubner, J. P., Schanze, K. S., Bedlek, J., and Morris, M. J., "Pressure and Temperature Measurements with a Dual-Luminophore Coating," *Proceedings of the ICIASF99 Record*, Inst. of Electrical and Electronics Engineers, New York, 1999, pp. 18.1–18.8.

[5]Morris, M. J., Donovan, J., Kegelman, J., Schwab, S., and Levy, R., "Aerodynamic Applications of Pressure Sensitive Paint," *AIAA Journal*, Vol. 31, No. 3, 1993, pp. 419–425.

[6]Davies, A., Bedwell, D., Dunleavy, M., and Brownjohn, N., "Pressure Sensitive Paint Limitations and Solutions," *Proceedings of the 7th International Symposium on Flow Visualization*, 1995, pp. 11–21.

R. P. Lucht
Associate Editor

Effects of Vibrational Relaxation on Bow Shock Standoff Distance for Nonequilibrium Flows

A. F. P. Houwing,* S. Nonaka,† H. Mizuno,†
and K. Takayama‡
Tohoku University, Sendai 980-8577, Japan

I. Introduction

PREVIOUS work by Hornung[1] considered the dependence of the normalized shock standoff distance on the normalized dissociation rate immediately after the normal shock in the simple case of a diatomic gas with only one reaction. His work allowed the dissociative nonequilibrium effects on the flowfield to be correlated for this specialized case. More recently, Hornung and Wen[2] extended this previous work to complex gas mixtures with many species and many reactions and to correct the correlation so that the additional parameter of the normalized freestream kinetic energy is accounted for. For the cases that they were considering, dissociative effects dominated the flowfield behavior. However, at somewhat lower specific total enthalpies, vibrational nonequilibrium behavior is dominant and can affect the shock standoff distance in a manner that is analogous to the dissociation cases. Because of this, we have applied their analytic approach to the case where vibrational relaxation effects are important and use the theoretical predictions as a basis for correlating recent ballistic range data. Though the analysis can be extended to account for a nonequilibrium freestream upstream of the bow shock, we limit ourselves to an equilibrium freestream in the current work.

II. Theoretical Considerations

Following Hornung and Wen,[2] we consider the conditions on the stagnation streamline along the symmetry axis between the shock and the stagnation point. The momentum and energy equations for inviscid adiabatic flow along this streamline, in the shock's frame of reference, are given by

$$\mathrm{d}p + \rho u\,\mathrm{d}u = 0 \tag{1}$$

$$\mathrm{d}h + u\,\mathrm{d}u = 0 \tag{2}$$

respectively, where p, ρ, u, and h are the pressure, density, flow speed, and specific enthalpy, respectively. From these two equations, one obtains the following relationship between the changes in the pressure and the specific enthalpy:

$$\mathrm{d}p = \rho\,\mathrm{d}h \tag{3}$$

For the case of a molecular gas, for which the vibrational modes are in equilibrium with each other at a vibrational temperature T_{vib}, while the rotational and translational modes are in equilibrium with each other at a temperature T, the entropy change per unit mass is given by[3]

$$\mathrm{d}s = (1/T)\,\mathrm{d}e + (p/T)\,\mathrm{d}(1/\rho) + [(1/T_{\mathrm{vib}}) - (1/T)]\,\mathrm{d}e_{\mathrm{vib}} \tag{4}$$

where e is the internal energy per unit mass and e_{vib} is the internal energy per unit mass due to vibrational excitation. In the case of a mixture of M atomic and diatomic constituents, N of which are molecular species that have vibrational degrees of freedom, this equation can be generalized to give

$$\mathrm{d}s = \frac{1}{T}\,\mathrm{d}e + \frac{p}{T}\,\mathrm{d}\left(\frac{1}{\rho}\right) + \sum_{i=1}^{i=N} c_i \left(\frac{1}{T_{\mathrm{vib},i}} - \frac{1}{T}\right)\mathrm{d}e_{\mathrm{vib},i} \tag{5}$$

where the subscript i identifies the chemical species; c_i is the mass fraction of species i; $e_{\mathrm{vib},i}$ is the internal energy per unit mass of a molecular species due to its vibrational excitation; the diatomic species are identified by values of i, where $1 \le i \le N$; and atomic species are identified by values of i, where $(N+1) \le i \le M$.

From Eq. (3) and the relationship between the specific internal energy, the specific enthalpy, the pressure, and the density, the only entropy change that occurs along the stagnation streamline is that associated with vibrational excitation. That is,

$$\mathrm{d}s = \sum_{i=1}^{i=N} c_i \left(\frac{1}{T_{\mathrm{vib},i}} - \frac{1}{T}\right)\mathrm{d}e_{\mathrm{vib},i} \tag{6}$$

Considering the internal degrees of freedom, we note that each species will have specific internal energy of translation

$$e_{\mathrm{trans},i} = \tfrac{3}{2} R_i T \tag{7}$$

where R_i is the gas constant for species i. In addition, each of the molecular species will have specific internal energy of rotation

$$e_{\mathrm{rot},i} = R_i T \tag{8}$$

and specific internal energy of vibration

$$e_{\mathrm{vib},i} = \frac{R_i \theta_{\mathrm{vib},i}}{\exp(\theta_{\mathrm{vib},i}/T_{\mathrm{vib},i}) - 1} \tag{9}$$

where $\theta_{\mathrm{vib},i}$ is the characteristic temperature of vibration of diatomic species i. Using the relationship between specific enthalpy, specific internal energy, and pressure, the specific enthalpy is then given by

$$h = \left[\frac{3}{2}\sum_{i=1}^{i=M} c_i R_i + \sum_{i=1}^{i=N} c_i R_i\right] T + \sum_{i=1}^{i=N} c_i e_{\mathrm{vib},i} + \frac{p}{\rho} \tag{10}$$

Defining two mass-averaged gas constants, as follows

$$\bar{R}_{\mathrm{vib}} = \sum_{i=1}^{i=N} c_i R_i \tag{11}$$

$$\bar{R} = \sum_{i=1}^{i=M} c_i R_i \tag{12}$$

and assuming an ideal thermal equation of state, we can rewrite the specific enthalpy as

$$h = \left[\frac{5}{2} + \frac{\bar{R}_{\mathrm{vib}}}{\bar{R}}\right]\frac{p}{\rho} + \sum_{i=1}^{i=N} c_i e_{\mathrm{vib},i} \tag{13}$$

Received 3 May 1999; revision received 6 December 1999; accepted for publication 30 March 2000.

*Visiting Professor, Shock Wave Research Center, Institute of Fluid Science; currently Senior Lecturer, Faculty of Science, Department of Physics, Australian National University, Canberra, Australian Capital Territory 0200, Australia.

†Graduate Student, Shock Wave Research Center, Institute of Fluid Science.

‡Director, Shock Wave Research Center, Institute of Fluid Science.

From this last equation, we readily see that, because each value of c_i is fixed (no chemical reactions), the caloric equation of state is in the form

$$h = h(p, \rho, e_{\text{vib},i}) \tag{14}$$

Therefore, the change in the specific enthalpy is given by

$$\mathrm{d}h = \frac{\partial h}{\partial \rho}\mathrm{d}\rho + \frac{\partial h}{\partial p}\mathrm{d}p + \sum_{i=1}^{i=N} c_i \,\mathrm{d}e_{\text{vib},i} \tag{15}$$

From Eq. (3), this becomes

$$\mathrm{d}h = \frac{\partial h}{\partial \rho}\mathrm{d}\rho + \rho\frac{\partial h}{\partial p}\mathrm{d}h + \sum_{i=1}^{i=N} c_i \,\mathrm{d}e_{\text{vib},i} \tag{16}$$

Solving this to determine the change in density gives

$$\mathrm{d}\rho = \left[\left(1 - \rho\frac{\partial h}{\partial p}\right)\Big/\frac{\partial h}{\partial \rho}\right]\mathrm{d}h - \left[1\Big/\left(\frac{\partial h}{\partial \rho}\right)\right]\sum_{i=1}^{i=N} c_i \,\mathrm{d}e_{\text{vib},i} \tag{17}$$

As observed in previous work,[2] we note that the coefficient of dh is related to the frozen speed of sound a_f and that dh can be replaced by $-u\,\mathrm{d}u$, so that the Eq. (17) can be rewritten as

$$\frac{\mathrm{d}\rho}{\rho} = -\frac{u^2}{a_f^2}\frac{\mathrm{d}u}{u} - \left[1\Big/\left(\rho\frac{\partial h}{\partial \rho}\right)\right]\sum_{i=1}^{i=N} c_i \,\mathrm{d}e_{\text{vib},i} \tag{18}$$

where

$$a_f^2 = \left[-\frac{\partial h}{\partial \rho}\Big/\left(\frac{\partial h}{\partial p} - \frac{1}{\rho}\right)\right]$$

As noted in previous work,[2] because the frozen Mach number u/a_f after the normal shock is typically 0.2 or less, the first term will be small, which implies that, in the absence of vibrational excitation, the density is practically constant along the stagnation streamline. When vibrational excitation is important, and dissociation effects are negligible, the density change along the stagnation streamline is essentially governed by the vibration:

$$\mathrm{d}\rho_s \approx -\left\{\left[1\Big/\left(\frac{\partial h}{\partial \rho}\right)\right]\sum_{i=1}^{i=N} c_i \,\mathrm{d}e_{\text{vib},i}\right\}_s \tag{19}$$

where the subscript s indicates conditions directly behind the bow shock on the stagnation streamline. In a similar way to the previous work for the case of dissociation, we will use this approximation to relate the average density on the stagnation streamline to the rate at which energy is absorbed by vibrational excitation at the shock. We note that our expression for dρ_s in Eq. (19) is analogous to that given by Hornung and Wen[2] if their term $(\partial h/\partial c_i)\,\mathrm{d}c_i$ is replaced by our term $c_i\,\mathrm{d}e_{\text{vib},i}$. Therefore, we incorporate our expression for dρ_s into a normalized vibrational rate parameter, which is defined as follows:

$$\tilde{\Omega}_{\text{vib}} \equiv -\frac{2a}{\rho_s u_\infty}\left\{\left[1\Big/\left(\frac{\partial h}{\partial \rho}\right)\right]\sum_{i=1}^{i=N} c_i \frac{\mathrm{d}e_{\text{vib},i}}{\mathrm{d}t}\right\}_s \tag{20}$$

which has the physical significance of

$$\tilde{\Omega}_{\text{vib}} = \frac{\text{energy absorption rate by vibration}}{\text{input rate of free stream kinetic energy}}$$

Here a is the radius of the spherical forebody, ρ_s is the density directly behind the shock on the stagnation streamline, and u_∞ is the freestream speed in the shock-fixed reference frame. To determine the value of $\partial h/\partial \rho$ at the shock, we make use of Eq. (13), from which it is readily determined that

$$\left(\frac{\partial h}{\partial \rho}\right)_s = -\left[\frac{5}{2} + \frac{\bar{R}_{\text{vib}}}{\bar{R}}\right]\frac{p_s}{\rho_s^2} \tag{21}$$

Previous work[2] describes two approximate analytic methods to determine the shock standoff distance. One method is applicable when the density ρ_b at the stagnation point on the body is less than the equilibrium density ρ_e behind a normal shock. The second method is applicable when the density ρ_b at the stagnation point on the body is equal to the equilibrium density ρ_e behind a normal shock. A third, more general and more accurate, nonanalytic method has also been proposed in previous work[2] and will be the one we shall consider first. By the substituting of our vibrational rate parameter for Hornung and Wen's reaction rate parameter,[2] this method assumes that the density profile is given by

$$\frac{\rho - \rho_s}{\rho_e - \rho_s} = 1 - \exp\left[-\frac{2\tilde{\Omega}_{\text{vib}}\rho_s}{\rho_e - \rho_s}\frac{y}{\Delta}\right] \tag{22}$$

where y is the distance from the shock. Integrating this to determine the average as done in the previous work gives

$$\frac{\bar{\rho} - \rho_s}{\rho_e - \rho_s} = 1 + \frac{1}{2\tilde{\Omega}_{\text{vib}}\tilde{\Delta}}\left(\frac{\rho_e}{\rho_s} - 1\right)\left(\exp\left[-\frac{2\tilde{\Omega}_{\text{vib}}\tilde{\Delta}\rho_s}{\rho_e - \rho_s}\right] - 1\right) \tag{23}$$

where

$$\tilde{\Delta} = \tfrac{1}{2}(\Delta/a)(\rho_s/\rho_\infty) \tag{24}$$

is a normalized shock standoff distance, Δ is the nonnormalized standoff distance, and ρ_∞ is the freestream density. The normalized standoff distance is related to the density behind the shock and the average density along the stagnation streamline,[2] with

$$\tilde{\Delta} = L(\rho_s/\bar{\rho}) \tag{25}$$

where, for the case of axisymmetric flows, $L = 0.41$ and $\bar{\rho}$ is the averaged value of ρ along the stagnation streamline.

In our work, we solve Eq. (23) to find $\tilde{\Delta}$ for different values of $\tilde{\Omega}_{\text{vib}}$ by finding the zero of the following function:

$$f(\tilde{\Delta}) = \frac{\tilde{\Delta}}{L}\left(\frac{\rho_e}{\rho_e - \rho_s}\right) + \frac{1}{2\tilde{\Omega}_{\text{vib}}L}\left(\frac{\rho_e - \rho_s}{\rho_s}\right) \times \left[\exp\frac{-2\tilde{\Omega}_{\text{vib}}\tilde{\Delta}\rho_s}{\rho_e - \rho_s} - 1\right] - \frac{\rho_s}{\rho_e - \rho_s} \tag{26}$$

This is done numerically using the Newton–Raphson technique.

To find the zero of the function defined in Eq. (26), it is necessary to evaluate the vibration rate parameter $\tilde{\Omega}_{\text{vib}}$, which, in turn, requires the evaluation of the rate of increase in vibrational energy behind the shock. To do this, we make use of the vibrational rate equation[3]

$$\frac{\mathrm{d}e_{\text{vib},i}}{\mathrm{d}t} = \frac{e_{\text{vib},i}^{\text{eq}} - e_{\text{vib},i}}{\tau_i} \tag{27}$$

where $e_{\text{vib},i}^{\text{eq}}$ is the value that the specific internal energy of vibration would have if $T_{\text{vib}} = T$ and τ_i is the characterisitic vibrational excitation time of species i. This characteristic time is dependent on the molecular properties of species i and those of its collision partners, as well as being a function of pressure and temperature. To account for collisions with different species j, here τ_i is given via the following summation:

$$\frac{1}{\tau_i} = \sum_j \frac{1}{\tau_{ij}} \tag{28}$$

where τ_{ij} is the characteristic time for vibrationally exciting species i through collisions with species j, given by[4,5]

$$\tau_{ij} = (B/p_j)\exp\left[A_{ij}\left(T^{-\frac{1}{3}} - 0.015\mu_{ij}^{\frac{1}{4}}\right) - 18.42\right] \tag{29}$$

where, τ_{ij} is given in seconds, $B = 1.013 \times 10^5$ N·s/m^2, p_j is the partial pressure (in newton per square meter) of the perturbing species j, μ_{ij} is the reduced molecular mass of the colliding partners (in kilogram per kilomole), and A_{ij} is a parameter that depends on the properties of species i and j and is given by[4]

$$A_{ij} = 1.16 \times 10^{-3}\mu_{ij}^{\frac{1}{2}}\theta_{\text{vib},i}^{\frac{4}{3}} \tag{30}$$

where $\theta_{\text{vib},i}$ is the characteristic vibrational temperature (in Kelvin) of species i.

As discussed by Park,[5] there are at least four exceptions to Eqs. (29) and (30). In particular, collisions of NO molecules with

other NO molecules and collisions of CO, O_2, and N_2 with O atoms result in relaxation rates much faster than those given by these equations. In the current work, these exceptions will apply only if chemical dissociation effects are significant.

Using Eqs. (27–30), Eq. (23) can be solved numerically to give $\tilde{\Delta}$ as a function of $\tilde{\Omega}_{\text{vib}}$. If experimental data can be represented as points in $\tilde{\Delta}$–$\tilde{\Omega}_{\text{vib}}$ space, it will then be possible to test the validity of Eq. (23).

In addition to Eq. (23), simpler approximate analytic relationships between $\tilde{\Delta}$ and $\tilde{\Omega}_{\text{vib}}$ can be determined in the same way as done by Hornung and Wen.[2] To arrive at these approximate forms, we simply substitute our $\tilde{\Omega}_{\text{vib}}$ for their $\tilde{\Omega}$ in their Eqs. (1) and (2). This gives

$$\tilde{\Delta} \approx (1/\tilde{\Omega}_{\text{vib}})\left[-1 + (1 + 2L\tilde{\Omega}_{\text{vib}})^{\frac{1}{2}}\right] \tag{31}$$

for $\rho_b < \rho_e$, and

$$\tilde{\Delta} \approx (\rho_s/\rho_e)\left[L + (1/\tilde{\Omega}_{\text{vib}})(\rho_e/\rho_s - 1)^2\right] \tag{32}$$

for $\rho_b \approx \rho_e$.

III. Comparison of Theory with Experimental Results

To test the effectiveness of Eqs. (23), (31), or (32) for correlating shock standoff distances, we will use the experimental data produced by Nonaka et al.[6] These authors used a ballistic range facility to project models with spherical forebodies into stationary dry air at a temperature of 293 K. Their data are particularly suitable for examing the dependence of the shock standoff distance on vibrational relaxation because of the following reasons. First, the conditions upstream of the bow shock are at a sufficiently low temperature so that virtually all of the molecules are in the ground vibrational state. Second, in their experimental work, care was taken to ensure that the gas was free of contaminants, such as water or oil-pump vapours, which can affect the vibrational relaxation rates.

In the comparison of theory with experimental data, we need to select data for which chemical relaxation effects are negligible. The criterion adopted in selecting these data is that the chemical reaction rates should be sufficiently slow behind a normal shock so that the flow between the shock vertex and the body stagnation point is chemically frozen.

The data selected from Nonaka et al.,[6] according to this criterion are presented in Table 1, where the data are grouped according to the upstream value of the binary scaling parameter ρa. In Table 1, V is the flight speed of the projectile, and all other parameters are as defined earlier. The percentage errors for the measurement of Δ are also presented.

Table 1 Ballistic range data from Nonaka et al.[6]

V, km/s	a, mm	Δ/a	Error in Δ/a, %
	$\rho a = 1.0 \times 10^{-4}$ (kg/m^2)		
2.63	14	0.135	3.15
2.67	14	0.1345	2.68
2.93	15	0.1397	1.15
3.57	7	0.1251	3.96
3.85	7	0.1212	1.82
	$\rho a = 2.0 \times 10^{-4}$ (kg/m^2)		
2.56	14	0.137	1.90
2.63	14	0.1332	1.84
3.15	15	0.1287	4.97
3.25	7	0.1277	2.58
3.36	7	0.1285	2.53
3.64	7	0.1137	2.99
	$\rho a = 4.0 \times 10^{-4}$ (kg/m^2)		
2.50	15	0.1324	2.57
2.61	15	0.1328	1.05
3.19	7	0.1187	3.79
3.37	7	0.1163	1.63
3.49	7	0.1129	1.33
	$\rho a = 1.7 \times 10^{-3}$ (kg/m^2)		
2.44	15	0.1278	2.19
2.56	14	0.1243	2.09
3.16	7	0.104	4.31

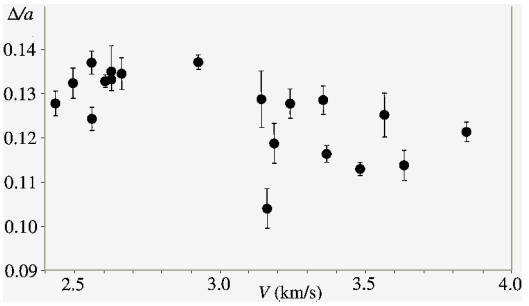

Fig. 1 Normalized standoff distance as a function of flight speed.

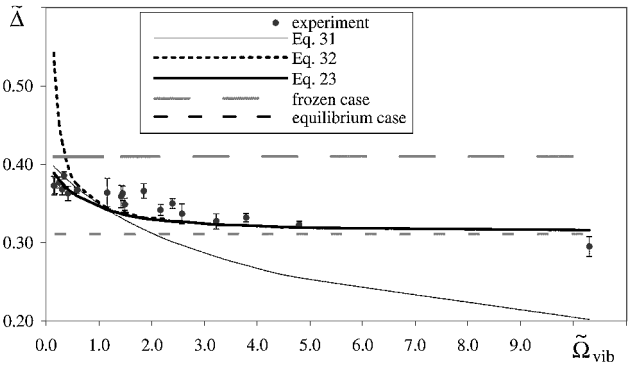

Fig. 2 Modified standoff distance as a function of vibrational rate parameter.

Figure 1 shows the data plotted in the Δ/a–V plane. As can be seen from Fig. 1, it is not possible to establish any correlation with the data plotted in this manner.

In Fig. 2, we present the same data in the $\tilde{\Delta}$–$\tilde{\Omega}_{\text{vib}}$ plane, where we see that the data collapse in a manner that suggests that $\tilde{\Delta}$ is a single-valued function of $\tilde{\Omega}_{\text{vib}}$. In Fig. 2, we have also plotted the perfect gas prediction, calculated from the ideal gas equations for a ratio of specific heats $\gamma = 1.4$, plus the solutions to Eqs. (23), (31), and (32). For the solutions of these equations, the conditions behind the normal shock and, in particular, the value for the density ρ_s were determined using a value of 1.4 for γ. The equilibrium value of the density ρ_e was determined by using a value of 1.2857 for γ, which corresponds to the case where all vibrational modes are excited.

Note that the solutions to Eqs. (31) and (32) cross at $\tilde{\Omega}_{\text{vib}} \approx 1$, whereas that of Eq. (23) follows one curve for $\tilde{\Omega}_{\text{vib}} < 1$ and the other curve for $\tilde{\Omega}_{\text{vib}} > 1$, as expected. It is only the curve of the solutions to Eq. (23) that is valid for the entire range of $\tilde{\Omega}_{\text{vib}}$ shown, and it is the one against which we shall make the experimental comparisons.

We note that the theory predicts the experimental results reasonably well, though the value of $\tilde{\Delta}$ is underpredicted in the range of $1 < \tilde{\Omega}_{\text{vib}} < 2.5$. In Fig. 2, we have included one result for which reactions are starting to become important. At the value of $\tilde{\Omega}_{\text{vib}}$ for this result ($\tilde{\Omega}_{\text{vib}} \approx 10$), the experimental value of $\tilde{\Delta}$ falls below the theoretical prediction. Because the analysis presented here is only valid in the absence of chemical reactions, this is expected. In fact, one would expect that $\tilde{\Delta}$ becomes smaller as a result of dissociation, in agreement with our observations.

In Fig. 2, we have also plotted the predicted values of $\tilde{\Delta}$ for the limiting cases of vibrationally frozen flow ($\tilde{\Delta} = 0.41$) and vibrational equilibrium flow ($\tilde{\Delta} = 0.31$) for the strong shock limit. These values were obtained from Eq. (25) putting $\bar{\rho} = \rho_s$ for the case of frozen flow and $\bar{\rho} = \rho_e$ for equilibrium flow.

IV. Conclusions

We have modified the theoretical analysis describing the dependence of the shock standoff distance on a sphere so that it is applicable to cases where vibrational relaxation behind the bow shock is important and chemical dissociation effects are negligible. The theoretical predictions have been compared with data produced in ballistic range experiments, and good agreement has been

observed. The analysis described here is particularly important in that it demonstrates which flow parameters are most suitable for the correlation of experimental data and allow standoff distances to be estimated quickly without the need to run time-consuming computational fluid dynamics codes, though such codes should be used to provide more detailed information where required.

Acknowledgments

The authors wish to thank H. Ojima and T. Ogawa for their assistance in conducting the experimental work described in the paper by Nonaka et al. (Nonaka, S., Mizuno, H., and Takayama, K., "Ballistic Range Measurement of Shock Shapes in Intermediate Hypersonic Regime," AIAA Paper 99-1025, Jan. 1999).

References

[1]Hornung, H. G., "Non-Equilibrium Dissociating Nitrogen Flow over Spheres and Circular Cylinders," *Journal of Fluid Mechanics*, Vol. 53, 1972, pp. 149–176.

[2]Hornung, H. G., and Wen, C.-Y., "Non-Equilibrium Dissociating Flows over Spheres," AIAA Paper 95-0091, Jan. 1995.

[3]Vincenti, W. G., and Kruger, C. H., *Introduction to Physical Gas Dynamics*, Wiley, New York, 1965, pp. 198–206.

[4]Millikan, R. C., and White, D. R., "Systematics of Vibrational Relaxation," *Journal of Chemical Physics*, Vol. 39, No. 12, 1963, pp. 3209–3213.

[5]Park, C., *Non-Equilibrium Hypersonic Aerothermodynamics*, Wiley, New York, 1990, pp. 56–60.

[6]Nonaka, S., Mizuno, H., and Takayama, K., "Ballistic Range Measurement of Shock Shapes in Intermediate Hypersonic Regime," AIAA Paper 99-1025, Jan. 1999.

M. Sichel
Associte Editor

Centerline Vorticity Transport Within a Jet in Crossflow

Václav Kolář*
Institute of Hydrodynamics,
166 12 Prague 6, Czech Republic
and
Eric Savory† and Norman Toy‡
University of Surrey,
Guildford, England GU2 5XH, United Kingdom

Introduction

THE single circular jet issuing normally into a crossflow (JICF) represents one of the basic jet-flow configurations with a wide variety of practical applications. These range from the aerodynamics of advanced short takeoff and landing (ASTOVL) aircraft and jet steering systems, through combustion chamber mixing, to environmental flows. Margason[1] provides an extensive survey of JICF studies during the past 50 years up to 1993 and recent papers, e.g., Smith and Mungal,[2] have shed a new light on the JICF problem as well. Though many aspects of the JICF including vorticity distributions (e.g., Refs. 3 and 4) have been treated in the literature, some aspects, such as the turbulent vorticity transport and the associated vortex strength decay of the well-known contrarotating vortex pair (CVP), still need to be clarified.

The aim of the present contribution has been to carry out the measurement of velocity fields and turbulence statistics in such a manner as to be able to visualize the centerline vorticity transport across the plane of symmetry (which is supposed to be the main cause of the cancellation of the vortex strength of the CVP) and to analyze the corresponding circulation decay rate directly in terms of the Reynolds stresses. Decay rates are closely associated with the effective turbulent vorticity fluxes defined in a manner similar to that in previous work[5] and determined by an analogous method as introduced by Kolář[6] for the planar case.

It is well recognized that large-scale organized vortical structures may exist within the flow field.[7] However, in the present work these are not taken into account and are reflected only as an inherent contribution to the long-time-averaged values of relevant quantities (denoted by angular brackets $\langle \cdots \rangle$).

Experimental Details

The measurements were carried out in a wind tunnel in the Department of Civil Engineering at the University of Surrey, using the standard crossed hot-wire anemometry technique. The tunnel working cross section was 0.62 m wide $\times$ 0.75 m high, and the jet nozzle of diameter $D = 13$ mm was placed flush with the ground plane. The jet outlet velocity was $U_J = 53.0$ m/s, resulting in $Re_J \approx 4.6 \times 10^4$. Only one jet-velocity/crossflow-velocity ratio, $R = U_J/U_C$, was studied, namely the ratio $R = 8$. Hence, the crossflow velocity was set to be $U_C = 6.63$ m/s. Flow symmetry is assumed in order to reduce the range of measurements to a half-plane. The coordinate system is shown in Fig. 1 with the origin at the center of the jet exit.

The crossed hot-wire measurements were, whenever necessary, undertaken with a tilted probe that was approximately aligned with the preestimated mean flow direction and the Reynolds stresses of interest were reconstructed based on the decompositions in the manner of Cutler and Bradshaw[8] using four probe roll positions. In the present case there is no wall effect and the probe volume is relatively small in comparison with the flow structures being investigated. Hence, the gradient errors will be within the bounds found previously.[8]

The velocity fields, that is the projections of the velocity vectors, $(\langle u \rangle, \langle v \rangle, \langle w \rangle)$, in the planes $x = $Const., were determined in five equidistant rectangular cross sections located at $x/D = 10$, 12.5, 15, 17.5, and 20 with dimensions $z = 70$–250 mm ($z/D \approx$ 5.4–19.2), $y = 0$–100 mm ($y/D \approx 0$–7.7), and with a square measurement mesh having steps of 10 mm. In the four corresponding midplanes, some necessary additional measurements of Reynolds stress tensor components in the centerline region were taken as well.

Turbulent Vorticity Fluxes

The only vorticity component considered here is the dominant one, aligned with the crossflow direction x, denoted $\langle \omega \rangle$. Figure 2a shows $\langle \omega \rangle$ for the measured half of the CVP for $x/D = 15$ ($x/RD = 1.875$). The coordinate RD-scaling, adopted in Figs. 2 and 3, has been found as the most appropriate scaling for physical dimensions of the JICF.[2]

Following previous work,[5] the turbulent transport of the mean vorticity is characterized by the antisymmetric turbulent vorticity flux-density tensor, which can be expressed purely in terms of gradients of the Reynolds stress tensor components. Along the centerline there is only one generally nonzero component of turbulent vorticity flux-density *vector* associated with $\langle \omega \rangle$, namely the y component, which is responsible for the centerline vorticity exchange between the single vortices of the CVP. The y component of the so-called *effective*[5] (that is, having generally a nonzero effect on $\mathrm{D}\langle \omega \rangle / \mathrm{D}t$

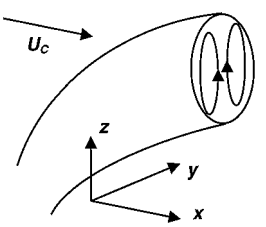

Fig. 1 Coordinate system.

Received 1 October 1999; revision received 28 April 2000; accepted for publication 1 May 2000.

*Senior Researcher, Academy of Sciences.

†Lecturer, Fluid Mechanics Research Group, Department of Civil Engineering.

‡Professor, Fluid Mechanics Research Group, Department of Civil Engineering.